Damage and fracture mechanisms in Ti-LCB and Ti-555 alloys : Micromechanical testing and modeling

P. Dufour[1], N. Clément[1], A. Lenain[2], T. Pardoen[1], P.J. Jacques[1]
[1]*Institute of mechanical, materials and civil engineering, Université catholique de Louvain, Place Sainte Barbe 2, B-1348 Louvain-la-Neuve, Belgium*
[2] *Techspace Aero, Route de Liers, 121, B-4041 Herstal, Belgique*

Abstract

New generations of β metastable and α/β titanium alloys are starting to replace the classical TiA6V4 alloy in many aeronautic structural components. The damage and fracture resistance of these alloys is not yet properly characterized and understood, which limits the reliability of the structural integrity assessment analysis as well as the optimization of the microstructures. Mechanical tests have been performed under different loading conditions, from tensile tests on notched and un-notched bars, on samples obtained with different thermomechanical routes and involving different volume fraction, morphology, and distribution of the α phase.

1. Introduction

A great interest has recently been given to titanium alloys due to their wide range of applications in medical, automotive and aerospace industries. For some applications, titanium alloys are key materials with their high performance to density ratio, allowing weight reduction to struggle CO_2 emissions. They are indeed more and more used for structural applications where they can bring a weight reduction that can reach 40%, while keeping the same mechanical resistance. Furthermore, the β-metastable alloys start to replace other α and α + β alloys since they present higher levels of specific strength [1]. The β metastable alloys present a sufficiently large $[Mo]_{eq}$ that allows avoiding the martensitic transformation to α' and α'' during quenching. The β phase can thus be entirely retained at the room temperature. In order to improve the properties of the material, further controlled ageing treatments are then carried out, giving a wide range of microstructures and a large variation of the resulting mechanical properties [2].

This study deals with the β-metastable TIMET Ti-LCB and Ti-555 alloys. Despite some studies on their mechanical properties, the mechanisms of damage and fracture remain mainly unknown while they constitute the design parameters for applications such as landing gears [3]. The influence of the stress-state on the mechanical response of several microstructures of Ti-555 and Ti-LCB is therefore compared to the classical Ti6Al4V in the present study.

The experimental measurements are compared to the prediction of a ductile fracture model in order to validate the behaviour of titanium alloys under static loading conditions.

2. Materials and microstructures

The chemical compositions and the transus temperature of the Ti-LCB and Ti-555, are given in Table I, while Table II shows the classification with respect to other common titanium alloys.

(wt.%)	Ti-555	Ti-LCB
Al	5	1.5
Mo	5	6.8
V	5	-
Cr	3	-
Fe	0.3	4.5
T_β (°C)	865	810

Table I. Chemical composition of the Ti-555 and Ti-LCB

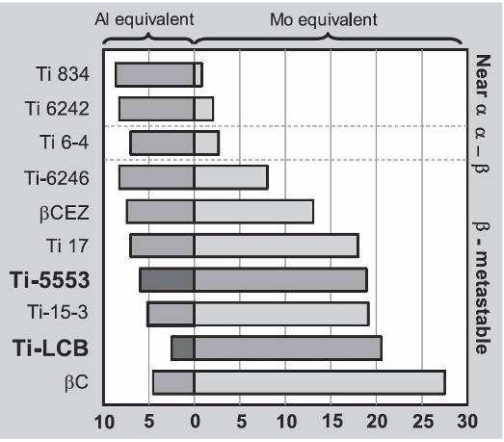

Table II. Classification of some titanium alloys according to their $[Mo]_{eq}$ and $[Al]_{eq}$ contents.

Different microstructures presented in Fig. 1 were obtained based on these alloys. Firstly, a fully β microstructure has been obtained by a solution treatment above the T_β temperature followed by water quenching in order to avoid the precipitation of the α phase. The Ti-555 was held at 875°C for 40 min, see Fig. 1 (a). An α-β microstructure, shown in Fig. 1(c), with only a few α nodules was generated with the Ti-LCB alloy at the end of an annealing at 815°C for 10 min. The bimodal microstructures shown in Fig. 1(b) and Fig. 1(d) were obtained at the end of two ageing steps after the solutionising, the first one at high temperature (820°C for 2 hours for the Ti-555 alloy and 760°C for 30 minutes for Ti-LCB alloy), bringing about large nodules of α inside the β grains and a quasi-continuous α layer along the β grain boundaries, and the second one at lower temperature bringing about a fine distribution of lamellae of α (630°C for 8 hours for Ti-555 and 538°C for 6 hours for Ti-LCB). Finally, the TA6V alloy presents relatively large nodules of α, see Fig. 1(e).

Several sample geometries were used, in order to investigate the influence of the stress-state on the ductility. Cylindrical smooth specimens were prepared from plates for uniaxial tensile tests while cylindrical specimens with an axisymmetric notch characterized by radii of curvature of either 1, 2 or 4 mm were machined for constant stress triaxiality tensile tests. The geometry of these specimens is shown on Fig. 2. For Ti-555 specimens, the tensile axis was perpendicular to the rotary

forging axis, resulting in the loading axis being perpendicular to the largest dimension of the grains. For the Ti-LCB specimens, the loading axis was parallel to the rod axis.

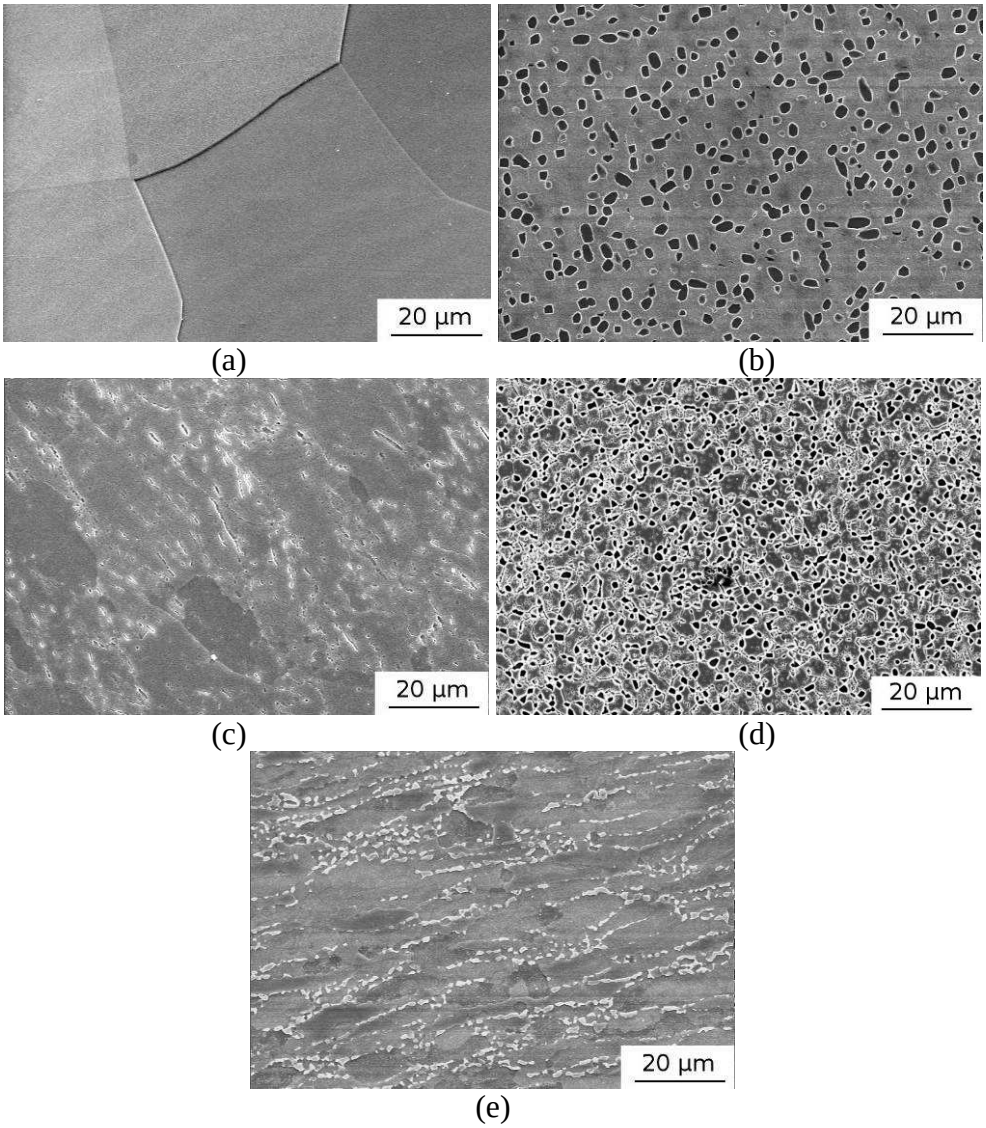

Fig. 1. SEM micrographs of the various alloys: (a) β Ti-555, (b) bimodal Ti-555, (c) low α Ti-LCB, (d) bimodal Ti-LCB and (e) TA6V.

The reduction in diameter at the minimum cross-section of the notched specimens was continuously measured by means of a radial extensometer. In all cases, both the initial and final diameters of the narrowest section were also measured using a travelling microscope in order to correct for errors due to the inaccurate initial positioning of the extensometer, which is never perfectly located at the minimum cross-section. Three tests were performed for each specimen geometry and microstructure.

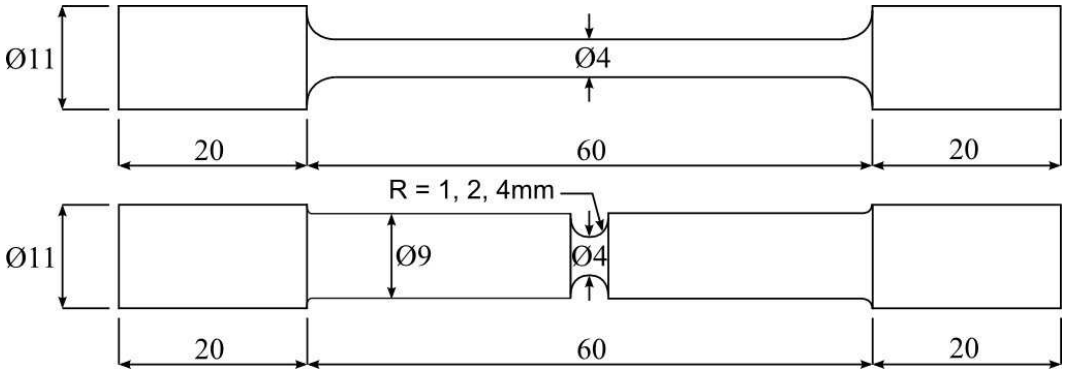

Fig. 2. Schematic illustration of the smooth and notched tensile samples

3. Results and Discussion

Fig. 3 presents the true stress - true strain curves of the notched and smooth specimens for the five alloys. Continuous measurements were carried out up to the maximum stress while the final stresses and strains indicated by a dot correspond to the last recorded load and the strain extracted from the final diameter on the broken sample.

As it can be seen on Fig. 3, an increase of the stress triaxiality brings about a large decrease of the ductility and an apparent increase of the yield strength. The only case that surprisingly does not respect this trend is the bimodal Ti-555, which presents a low ductility at low stress triaxiality.

The comparison of these tensile curves shows that the best ductility is achieved for the low α Ti-LCB, probably partly thanks to a smaller grain size. Contrarily, the bimodal Ti-555 presents a very low ductility.

Fig. 4 presents low magnification micrographs of the fracture surfaces of different samples of Ti-555. The fracture surfaces of the β sample (Fig. 4(a) and (b)) are characterized by smaller facets than for the bimodal sample (Fig. 4(c) and (d)), in which large elongated facets can be observed. The faceted surface indicates intergranular fracture modes. This can be explained by the shape of the grains: very large and elongated grains perpendicular to the loading direction for the bimodal samples, which are smaller and equiaxed after recrystallization in the β samples. Furthermore, the high triaxiality results show a more pronounced height difference between the facets.

Fig. 5 shows that the fracture surfaces of the Ti-LCB and TA6V alloys do not present the large scale features observed in the bimodal Ti-555.

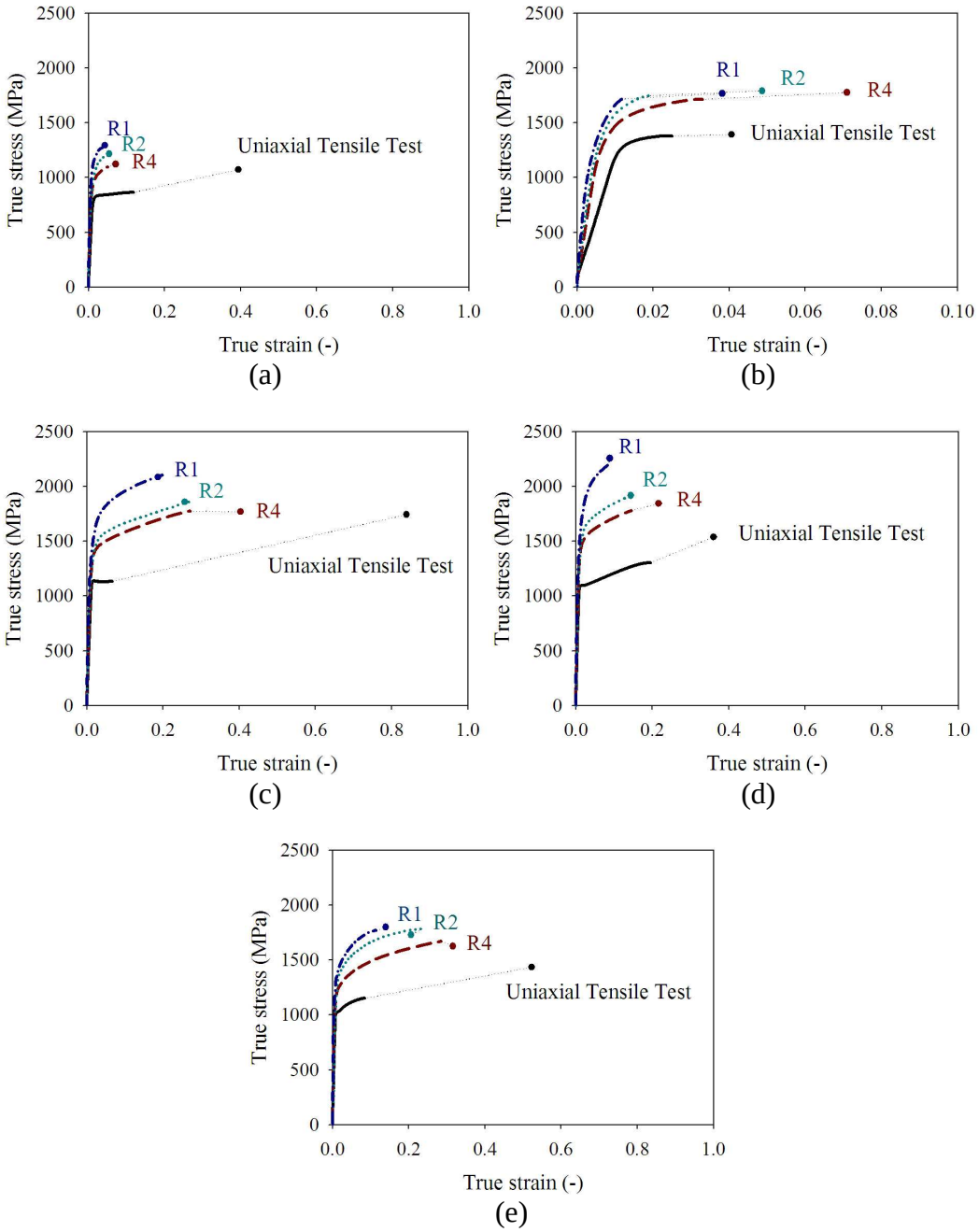

Fig. 3. True stress – true strain curves of the different samples tested with smooth and notched samples; (a) β and (b) bimodal microstructure of Ti-555, (c) low α Ti-LCB, (d) bimodal Ti-LCB, and (e) the classical Ti64. The bimodal Ti-555 graph (b) has a different abscise scale.

At larger magnification, all the microstructures present a fracture surface containing voids that are characteristic of a ductile mode of fracture whether it is intergranular or intragranular. Fig. 6 illustrates this observation in the case of the (a) Ti-555, (b) Ti-LCB and (c) TA6V.

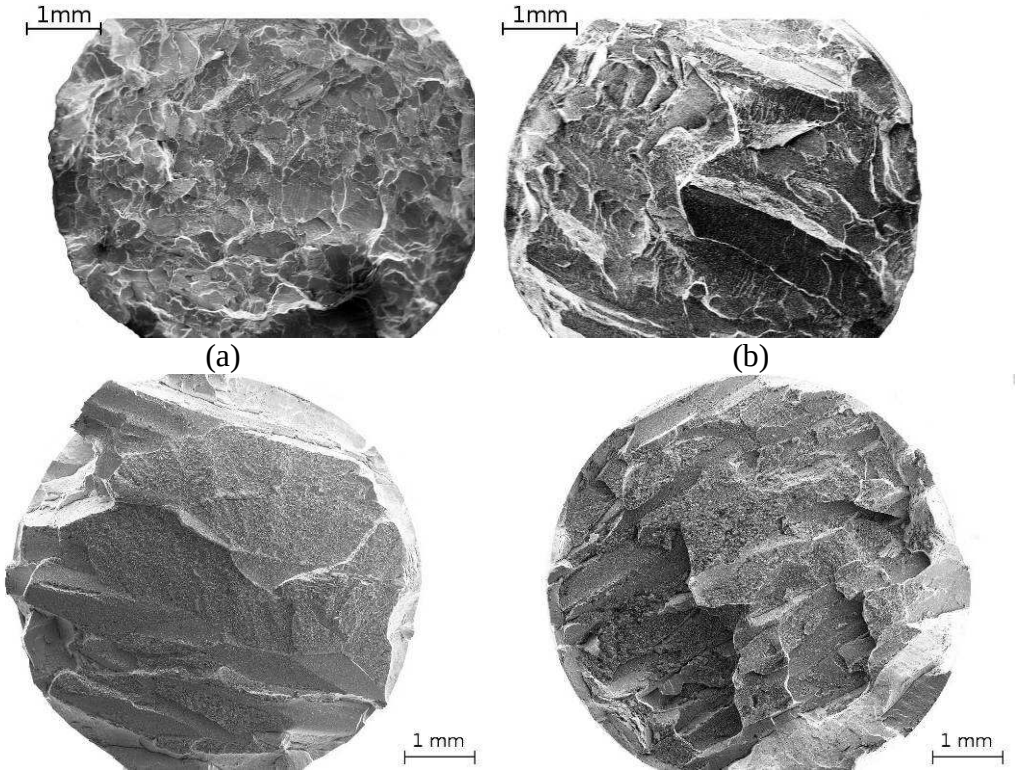

Fig. 4. Low magnification micrographs of the fracture surfaces of (a) β Ti-555 with low triaxiality (R4), (b) high triaxiality (R1), and bimodal Ti-555 (c) with low and (d) with high triaxility.

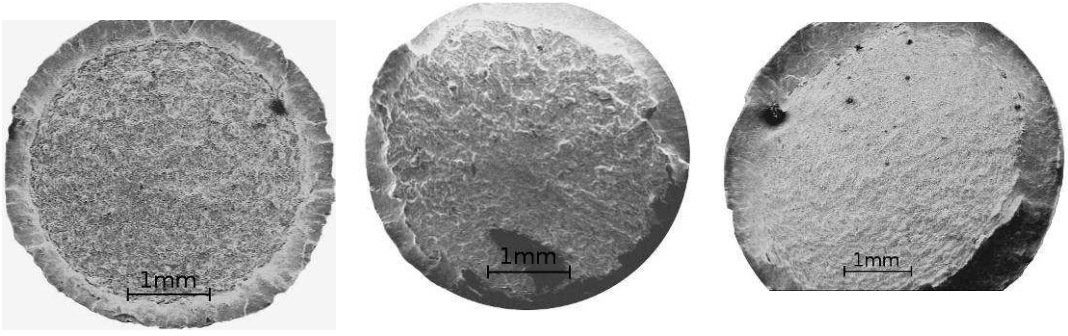

Fig. 5. Micrographs of the fracture surface of (a) the low α Ti-LCB, (b) bimodal Ti-LCB, and (c) TA6V.

Finally, Fig. 7 presents SEM micrographs of zones of the Ti-555 below the fracture surface on planes parallel to the loading direction. They reveal that α particles are always involved in the void nucleation. Furthermore, they confirm that the crack tends to follow the prior β grain boundaries as suggested by the observation of the fracture surfaces.

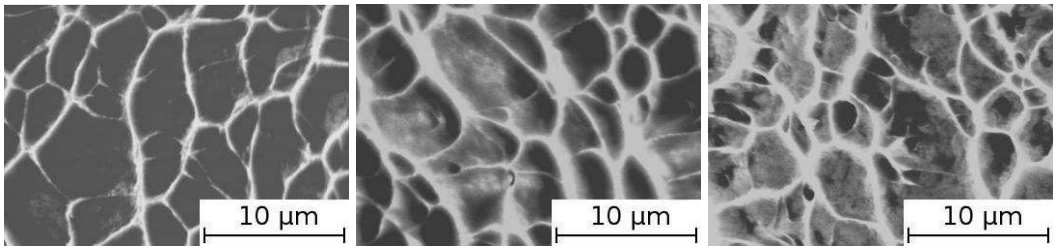

(a) (b) (c)

Fig. 6. Typical SEM micrographs of the fracture surface of (a) Ti-555, (b) Ti-LCB, and (c) TA6V, showing the presence of voids.

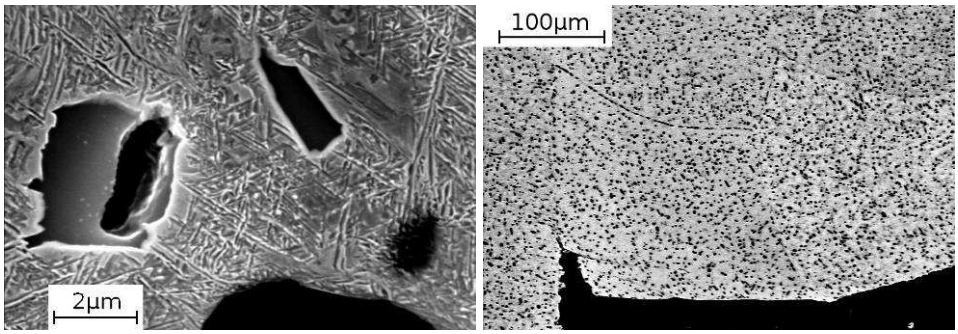

(a) (b)

Fig. 7. Damage in bimodal Ti-555; (a) void nucleated from α particles and (b) damage following a β grain boundary.

The experimental results are compared to a model based on the three steps of ductile fracture: void nucleation, growth and coalescence. Void nucleation is assumed to occur when the maximum principal stress $\sigma_{princ}^{p\max}$ in the particle or at the interface reaches the critical value σ_c :

$$\sigma_{princ}^{p\max} = \sigma_c^{bulk} \text{ or } \sigma_c^{\text{int}erface} \qquad \text{(Equ. 1)}$$

The maximum principal stress in the particle is related to the overall stress state $\sigma_{princ}^{\max}$, according to the Beremin model [4] :

$$\sigma_{princ}^{p\max} = \sigma_{princ}^{\max} + k_s\left(\sigma_e - \sigma_0\right) \qquad \text{(Equ. 2)}$$

where k_s is a parameter describing the shape of the particles, σ_e is the equivalent von Mises stress, and σ_0 is the yield stress.

The voids extend by a plastic growth rather than propagation by cleavage in the matrix. The void growth rate mechanism is described by the Rice and Tracey model [5] :

$$\frac{dR}{R} = \alpha \exp\left(\frac{3}{2}T\right) d\bar{\varepsilon}^{p} \qquad \text{(Equ. 3)}$$

where R is the radius of the void and $\bar{\varepsilon}^p$ is the equivalent plastic strain.

Finally, the onset of void coalescence is predicted by the Thomason criterion [6], which writes

$$\frac{\sigma_z}{\sigma_y} = \left(1-\chi^2\right)\left[\alpha\left(\frac{1-\chi}{\chi W}\right)^2 + \beta\sqrt{\frac{1}{\chi}}\right] \qquad \text{(Equ. 4)}$$

where α and β are parameters depending of the strain hardening, χ is the relative void spacing and W is the void aspect ratio. More details about the evolution law used for W and χ are given in Ref[7].

The Thomason criterion states that coalescence occurs when the stress normal to the localisation plane reaches a critical value that decreases as the voids open (W increases) and get closer to each other (χ increases).

The unknown parameters of the model, i.e. the void nucleation stress σ_c, the initial relative void spacing χ_0 and the parameter k_s are determined by inverse identification on a subset of experimental data.

Fig. 8 compares the experimental values and the predicted ductilities for different stress triaxialities and different microstructures. The dashed curves represent the critical nucleation strain and the solid curves represent the fracture strain. Experimental measurements are indicated by the dots.

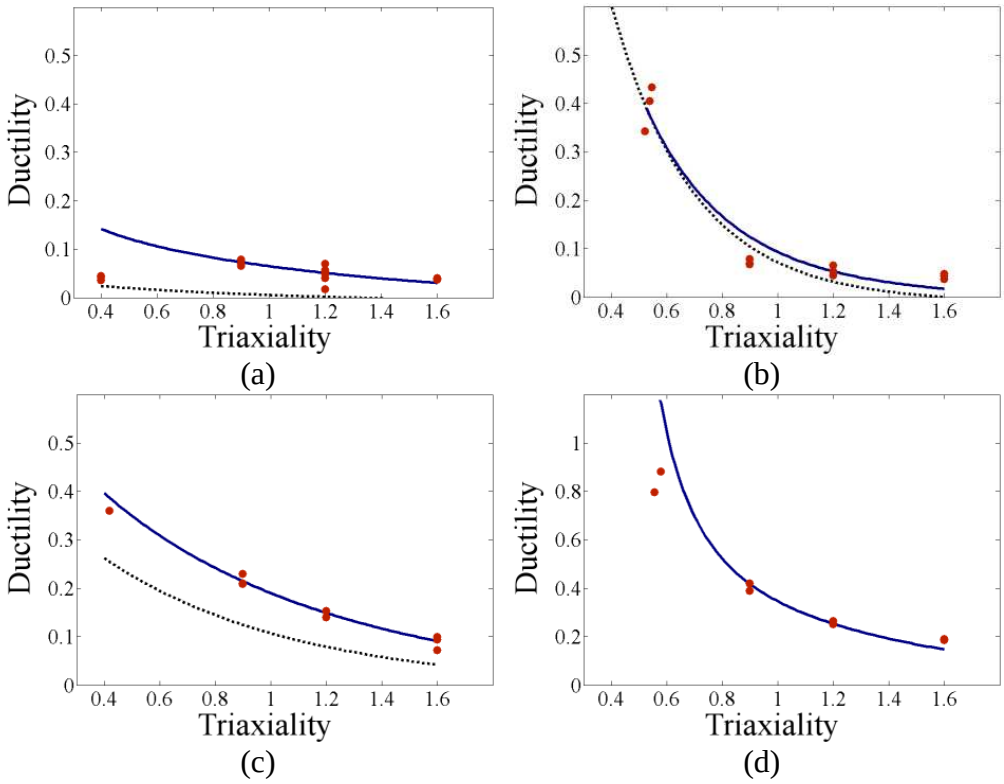

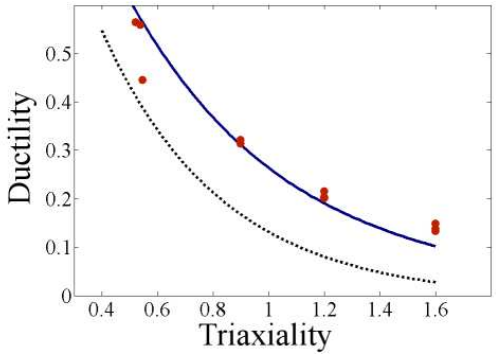

(e)

Fig. 8. Comparison of the modelled fracture strain and the experimental results for (a) the β Ti-555, (b) the bimodal Ti-555, (c) the low α Ti-LCB, (d) the bimodal Ti-LCB and (e) the TA6V.

The predicted fracture strains match quite well with the experimental values, except for the bimodal Ti-555. For this microstructure, the fracture strain drops at low triaxiality (for the uniaxial tensile tests) which is something that any similar ductile damage model will never be able to capture. This particular behaviour results from the presence of weak zones in these samples. As shown on Fig. 7(b), the fracture is intergranular, following the larger density of α particles along the prior β grain boundaries.

4. Conclusion

The ductile fracture of some microstructures of Ti-555, Ti-LCB and TA6V has been investigated. It has been shown that low α Ti-LCB presents the best ductility while the ductility of bimodal Ti-555 is very low due to an intergranular ductile fracture. The model captures relatively well the influence of triaxiality on the studied microstructures except for the bimodal Ti-555 where the presence of weak zones drastically affects the fracture of smooth specimens involving large volume of material undergoing high stress levels. The damage evolution on this latter microstructure has to be investigated, as well as for the β Ti-555 who presents very low ductilities for high triaxialities. *In situ* micromechanical tests will soon be carried out for this purpose. The influence of the stress triaxiality on the ductility of some other microstructures of the Ti-555 will be investigated as well.

5. Acknowledgments

The authors would like to express their acknowledgements to TIMET Savoie for provision of the Ti alloys. The work of A. Lenain and P. Dufour was supported by a grant from F.R.I.A., Belgium. Financial support from Région Wallonne through the RW-WINNOMAT I program under convention TITAERO 41/5659 is gratefully acknowledged. This research has also been carried out under the interuniversity attraction poles program P6/24, funded by the Belgian State, Belgian Science Policy.

6. References

[1] J.C. Fanning, S.P. Fox, Recent Developments in Metastable β Strip Alloys, JMEPEG 14 (2005) 703-708

[2] S. Ankem, C.A. Greene, Recent developments in microstructure/property relationships of beta titanium alloys, Materials science and engineering A263 (1999) 127-131

[3] J.C. Fanning, R.R. Boyer, Properties of Timetal 555 - A new near-beta titanium alloy for airframe components, in : Ti-2003 Science and Technology, Luetjering, Gerd / Albrecht, Joachim (eds.), WILEY-VCH Verlag GmbH & Co. KGaA, Germany, 2004, pp. 2643-2651

[4] F. M. Beremin, Cavity formation from inclusions in ductile fracture of A508 steel, Metallurgical Transactions A 12 (1981), 723-731

[5] J. R. Rice, G. F. Rosengren, On the ductile enlargement of voids in triaxial stress, Journal of Mechanical and Physical Solids 17 (1969), 210-217

[6] P. F. Thomason, 1990, Ductile Fracture of Metals, Pergamon, Oxford, 1990

[7] D. Lassance, F. Scheyvaerts, T. Pardoen, Growth and coalescence of penny-shaped voids in metallic alloys, Engineering Fracture Mechanics 73 (2006), 1009-1034